Diesel, Spark-Ignition, and Turboprop Engines for Long-Duration Unmanned Air Flights

Daniele Cirigliano,* Aaron M. Frisch,† Feng Liu,‡ and William A. Sirignano‡
University of California, Irvine, California 92697

DOI: 10.2514/1.B36547

Comparisons are made for propulsion systems for unmanned flights with several hundred kilowatts of propulsive power at moderate subsonic speeds up to 50 h in duration. Gas-turbine engines (turbofans and turboprops), two- and four-stroke reciprocating (diesel and spark-ignition) engines, and electric motors (with electric generation by a combustion engine) are analyzed. Thermal analyses of these engines are performed in the power range of interest. Consideration is given to two types of generic missions: 1) a mission dominated by a constant-power requirement, and 2) a mission with intermittent demand for high thrust and/or substantial auxiliary power. The weights of the propulsion system, required fuel, and total aircraft are considered. Nowadays, diesel engines for airplane applications are rarely a choice. However, this technology is shown to be a very serious competitor for long-duration unmanned air vehicle flights. The two strongest competitors are gas-turbine engines and turbocharged four-stroke diesel engines, each type driving propellers. It is shown that hybrid-electric schemes and configurations with several propellers driven by one power source are less efficient. At the 500 KW level, one gas-turbine engine driving a larger propeller is more efficient for durations up to 25 h, whereas several diesel engines driving several propellers become more efficient at longer durations. The decreasing efficiency of the gas-turbine engine with decreasing size and increasing compression ratio is a key factor.

Nomenclature

A_{inj}	=	injector cross-sectional area
B	=	cylinder bore
C_D	=	discharge coefficient
C_P	=	power coefficient
C_T	=	thrust coefficient
h	=	heat transfer coefficient
J	=	advance ratio
L	=	cylinder stroke
m	=	cylinder content mass
m_{air}	=	air mass
m_b	=	burned zone mass
m_c	=	chamber mass
m_f	=	fuel mass
$\dot{m}_{\text{inj}}$	=	fuel flow through the injector
m_u	=	unburned zone mass
$\mathcal{P}$	=	power
p_c	=	chamber pressure
p_{cc}	=	crankcase pressure
Q	=	heat energy
Q_{ch}	=	energy released by combustion
Q_{ht}	=	energy lost by heat transfer to the walls
Q_{sens}	=	sensible energy
R_b	=	Boltzmann constant of burned gas
R_u	=	Boltzmann constant of unburned gas
$\mathcal{T}$	=	thrust
T_b	=	temperature of burned zone
T_c	=	chamber temperature
T_{cc}	=	crankcase temperature
T_u	=	temperature of unburned zone
T_w	=	cylinder walls temperature
U	=	internal energy
V_b	=	burned zone volume
V_c	=	chamber volume
V_{cc}	=	crankcase volume
V_u	=	unburned zone volume
W	=	work energy
$\mathcal{W}$	=	weight
x_b	=	mass fraction burned
α	=	air–fuel ratio
γ_b	=	specific heat ratio of burned zone
γ_c	=	specific heat ratio of compression stroke
γ_e	=	specific heat ratio of expansion stroke
ε	=	cylinder compression ratio
η_c	=	compressor adiabatic efficiency
η_{th}	=	thermal efficiency
θ	=	crank angle
τ_c	=	compressor temperature ratio
τ_t	=	turbine temperature ratio

Received 16 November 2016; revision received 24 October 2017; accepted for publication 7 November 2017; published online 27 December 2017.

*Graduate Exchange Student, Aeronautical Engineering, Politecnico di Milano, Italy; currently Aeronautical Engineer, Operations Management Leadership Program, Avio Aero, a GE Aviation Business Via I Maggio, 99, 10040 Rivalta di Torino (TO), Italy.

†Mechanical Design Engineer, Aerojet Rocketdyne, Canoga Park, CA; currently Mechanical Engineer, Solar Array and Mechanisms Products, Lockheed Martin, Space Systems Company Sunnyvale, CA 94089.

‡Professor, Mechanical and Aerospace Engineering. Fellow AIAA.

I. Introduction

UNMANNED air vehicles (UAVs) that require several hundred kilowatts of power and flight durations of a day or longer typically use either gas-turbine engines or spark-ignition engines. Diesel engines have not been discussed widely in the literature, although they offer potential advantages. Although the gas-turbine engine suffers a decrease in efficiency as compression ratio increases and engine size decreases, the turbocharged diesel can maintain a higher efficiency. For longer flight durations, fuel weight becomes more dominant, and the weight disadvantage of diesel engines becomes less significant. In this research, we make generic comparisons between gas-turbine engines, spark-ignition engines, and diesel engines for long-duration UAV flights. The purpose is not to show superiority of diesel engines for any specific real mission. Rather, by examination of several sample generic missions described simply by duration, power requirements, and cruise altitude, the competitiveness of the diesel engine is demonstrated. Thereby, the designer of a UAV for a specific mission is provided enough information to know that diesel engines are options deserving detailed examination.

The scaledown of gas-turbine engines results in decreased efficiency because of certain scale effects: profile losses, end-wall losses, Reynolds number effects, heat transfer, and tip clearance losses. Frisch [1] finds that, at very low size and power (inlet diameter below 10 cm and 300 kW), the gas-turbine engine efficiency becomes too low. It is

Table 1 Examples of existing high-altitude UAVs

UAV	Power	Ceiling, kft	Cruise/maximum speed, kt	Fuel/payload, kg	Endurance, h
Predator MQ-1 GA (1995)	Rotax 914, four-cylinder, four-stroke, 101 hp	25	90/117	— —	35
Reaper MQ-9 (2001)	Honeywell TPE331-10 turboprop, 900 hp (671 kW)	50	169/260	— —	— —
Predator C a.k.a. Avenger (2009)	Pratt & Whitney Canada, PW545B turbofan, thrust 3991 lbf	50	350/400	3600/1600	18
Predator C extended wing (Oct. 2016)	Pratt & Whitney Canada PW545B turbofan, thrust 3991 lbf	50	350/400	4600/1400	20
Global Hawk Northrop (1998)	Rolls-Royce F137-RR-100 turbofan engine, 7600 lbf	60	310/340	14,600 gross	36

conceivable that, at some point, it can be replaced by another source of power, such as an internal combustion (IC) engine. The Diesel cycle is theoretically more efficient than the Otto cycle, given the higher compression ratios and lean-burn combustion. Hence, a diesel engine may be the best candidate for this purpose, resulting in the same amount of power generation yet at a higher efficiency.

UAVs are often used in long missions, like reconnaissance flights. Current technology allows these planes to fly at altitudes up to 25,000 ft, but some reconnaissance UAVs are able to fly up to 50,000 ft in the near future [2]. Some examples are shown in Table 1. Data are taken from [3–5]. For mid-to-long mission durations, perhaps tens of hours, the reciprocating engine is likely the best candidate to drive the aircraft because of its higher efficiency (i.e., lower fuel consumption) compared to a gas-turbine engine of the same power [6].

For engine–propeller coupling, it is theoretically possible to have an engine driving a propeller directly, several propellers driven by one single engine by means of mechanical connections, or electrical motors with electricity produced onboard. The best choice among these must be evaluated. Hence, the scope of this work is to determine under which conditions of core size and power the gas turbine engine can be replaced with another power source, resulting in the same amount of power yet at a higher efficiency. The target is to determine the most efficient power source in the range of 300–500 kW, to power a UAV flying at altitudes up to 20,000 ft for several hours. Moreover, the best engine–propeller coupling will be investigated.

II. Candidate Engines

In this study, many engine types have been investigated. Data on power, weight, and size have been collected from technical sheets available in open literature [7–13]. A wide range of power sources are considered, including reciprocating engines, turbine-based engines, and electric motors. The list of the engines sampled for this analysis is reported in Tables 2 and 3. Data sheets of all of these engines were examined and data concerning power, weight, and size were extracted. The electric motors reported in Table 3 do not include the thermal management system; more precisely, their weight is composed of the coils, the casing, and the shaft only.

Some of the automotive engines listed in the tables are not compatible with high-altitude operation, due to their weight, size, and piston configuration. Low-speed, medium-altitude capable systems should be designed to reduce weight and minimize volume. Plus, the low density and temperature of the air should be hindered by a proper turbocharging system. Finally, the pistons arrangement should be designed for propeller's balancing, smooth functioning, and efficiency; for example, in early 1900s, the "star configuration" (cylinders disposed radially with respect to propeller axis) was highly diffused. For these reasons, the engines reported in the aforementioned tables are taken just for comparison of their specifications.

Figure 1 shows the relation between weight and power for the different engines investigated. The diagram is a log-log plot with six orders of magnitude in the abscissa and in the ordinate. The engines tend to be organized along a straight line, or reference line, suggesting a power law in the form $W = a + bP^c$ (W = weight, P = power). Fitting curves have been optimized with the coefficients in Table 4. Although this approach can appear a bit cursory, it is the authors' opinion that it is accurate enough to support the rest of the paper. In fact, on a 100 kg engine, an error of ± 20 kg is acceptable in this context

Table 2 Sampled reciprocating engines designations

Two-stroke CI	Two-stroke SI	Four-stroke CI	Four-stroke SI
PF 4-53T (T)[a]	1VR-DF	MDI TC GD BS-II (T)	1.8 20vT (T)
PF 4-53N	120AX	NEF 2.6 BS-II (T)	5.2 V10 FSI
PF 3-53N	104RX	NEF 2.6 BS-III (T)	P86
PF 6V53T (T)	160RX	Ford V8 6.0 liter (T)	P80
PF 3-71N	55AX AB	Ford V8 6.4 liter (T)	P84
PF 4-71N	75AX ABL	Ford V8 7.3 liter (T)	P84/5
— —	— —	MBE900 (T)	P83
— —	— —	LD4B 3.9-60G (T)	8.0 W16 64V (T)
— —	— —	YC4108ZD (T)	BMW N63 (T)
— —	— —	YC4108ZC (T)	2.0 TFSI (T)
— —	— —	4JB1T-1 (T)	60 EPI Mercury
— —	— —	Centurion 1.7 (T)	Mercedes A200 (T)
— —	— —	— —	ROTAX 915 IS/ ISC

[a]T = turbocharged.

Table 3 Sampled turbine engines and electric motors designations

Turbofan	Turbojet	Turboprop	Electrical motors
ALF502H	JT12A-8	RR500	OSMG9505
AE-3007	JT8D-219	M250	OSMG9538
TAY 620	JT3C-7	AE-2100	Yuneec
BR710-A1	AL-7F	PT6B-37A	Hi-Pa Drive
CF34-10E	YJ93	M601D-1	— —
PW2037	J58	TPE331-43A	— —
JT-9D-7R4	F135-PW-100	Allison T56	— —
CF6-80C2	Olympus 593	GE H75	— —
GE 90	— —	RR300	— —
Trent 800	— —	— —	— —

because the fuel weight required for a mission longer than 10 h is in the order of thousands of kilograms, two orders of magnitude higher. The weights reported in Fig. 1 is the engine dry weight, which is important for the reciprocating engines; turbine engines weight comprehends the cooling system, although the electric motors are composed of the coils (rotor and stator), the casing, and the motor shaft only. Unfortunately, it is difficult to obtain precise information on the weight of an engine on a commercial data sheet; hence, a small degree of approximation, as explained before, must be used.

In Fig. 1, attention should be paid to the central part of the diagram. Commercial naturally aspirated engines of around 100 kW power deviate dramatically from the straight line; these engines follow the reference line only in the first part of the plot, between 0.1 and 30 kW; then, they diverge. In formula 1 engines, however, a deviation from the straight line comes above 300 kW for naturally aspirated engines larger than 300 kW in Fig. 1. This can be attributed to their large bore-to-stroke ratio (usually greater than 1) and the use of cutting-edge light materials. For a given power, turbocharged engines are generally heavier than their naturally aspirated counterpart, mostly because of the turbocharger itself.

Turboprop engines follow the straight line, but because of the architecture of the engine itself, they seem to be used only for

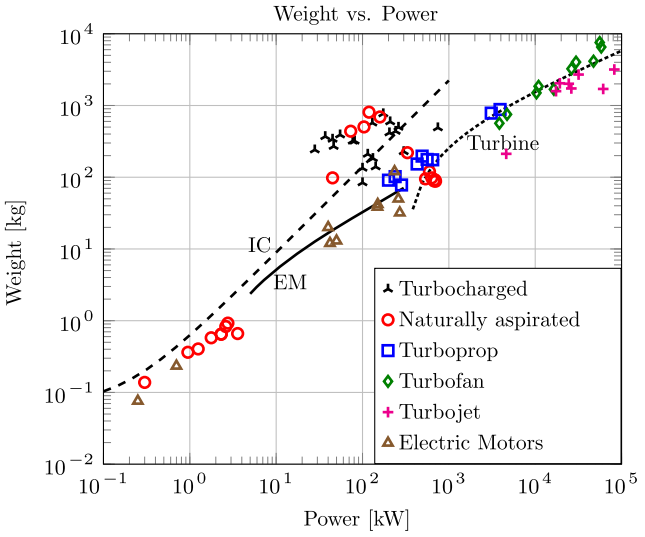

Fig. 1 Weight and power of the power sources investigated.

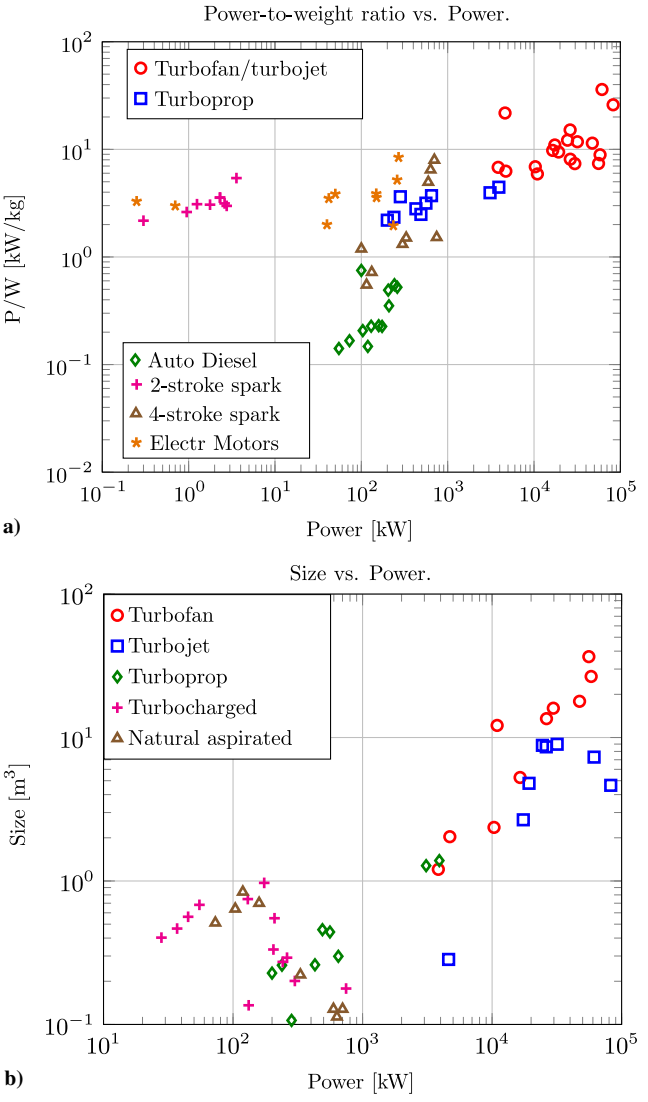

Fig. 2 Comparison of P/W and size between various existing engines.

applications over 100 kW. Turbofan and turbojet engines occupy the top-right part of the diagram. Both the categories are lower limited by 10^3 kW and reach easily 10^5 kW when high bypass turbofan and after-burning turbojet engines are involved. For the same power, however, turbojet engines are lighter. Turbofan engines suffer from the additional weight of the outer bypass channel and the large fan. The electric motors investigated are located on the reference line and can be manufactured in a large range of power: below 1 kW (e.g., for model airplanes), up to tens of kW. From the previous discussion, turbofan and turbojet engines are at a disadvantage for the purpose of this work, both for their weight and because they become inefficient below the range of interest, 300 kW.

Figure 2a shows the power-to-weight ratio versus power for every engine investigated in this work. On a P/W versus P map, it is desirable to obtain an engine as close as possible to the top. For the purpose of this work, we are also interested in the area near 10^2 kW. Here, we find the electric motors, which have the highest power-to-weight ratio. Because they do not need many mechanical parts to work, they are the lightest for a given power. Compression ignition (CI) engines for commercial vehicles have the lowest power-to-weight ratio, being generally heavier than spark ignition (SI) engines. Gasoline engines and turboprops stay in the middle and could also be used for the purpose of this work.

Data about the engine size have been collected as well and are shown in Fig. 2b. The model adopted for computing the size is the so called box size, meaning the maximum volume occupied by the machine. Turbofan engines are generally bigger than turbojets, due to the presence of the large front fan. Reciprocating engines are the most compact and occupy the bottom-left part of the diagram.

For a long-range reconnaissance UAV, the engine is expected to be efficient, light, compact, reliable, and not very noisy. For the considerations made thus far, the turbofan and turbojet engines are disadvantaged and therefore excluded from further considerations because they are inefficient at the 300 kW power level under examination in this paper. Also, an electric configuration is excluded, given the poor energy density of the batteries available nowadays. A typical energy density ranges between 0.6 and 0.8 MJ/kg, according to the current technology [12]. All other power sources will be tested to obtain a general idea of how suitable they are for our scope.

Table 4 Coefficients of the power-weight fitting curves in the form $W = a + bP^c$

Engine type	a	b	c	Power range, kW	R^2
IC engines	0.068	0.5608	1.2	0.1–1000	0.889
Turbine engines	−303.9	15.54	0.5188	300–10^5	0.918
Electric motors	−2.354	1.609	0.6693	5–300	0.832

A deeper analysis will focus on IC engines and on gas turbine engines coupled with an unshrouded propeller (also called turboprop).

The power target for this first analysis is 300 kW. (Later, higher powers will be studied.) This can be obtained in several ways: by only one 300 kW engine, two 150 kW engines in parallel, three of 100 kW, and so on. The choice of which one for minimum total aircraft weight is a main topic of this research.

III. Results

To assess the capabilities of a certain engine, a numerical code able to compute its properties, given its geometry and some boundary conditions, is needed. Five engine types have been selected, and a numerical Matlab code has been written for each one of them: four-stroke CI, four-stroke SI, two-stroke CI, two-stroke SI, and gas-turbine engine. The numerical codes are briefly discussed in Appendices A and B.

The five numerical codes are used to compute several properties of the engines, including thermal efficiency. Three flight altitudes are investigated: 10,000, 15,000, and 20,000 ft. The cruise flight Mach number is 0.4. The engine design allows for the following parameters to be modified in the numerical code of the reciprocating engine: equivalence ratio, engine rotation frequency, and engine size (bore, stroke, and number of cylinders).

In this study, the IC cylinder geometry (bore = 8 cm, stroke = 9 cm) is kept constant with altitude and power. A restriction to the efficiency-maximization process is that the equivalence ratio Φ

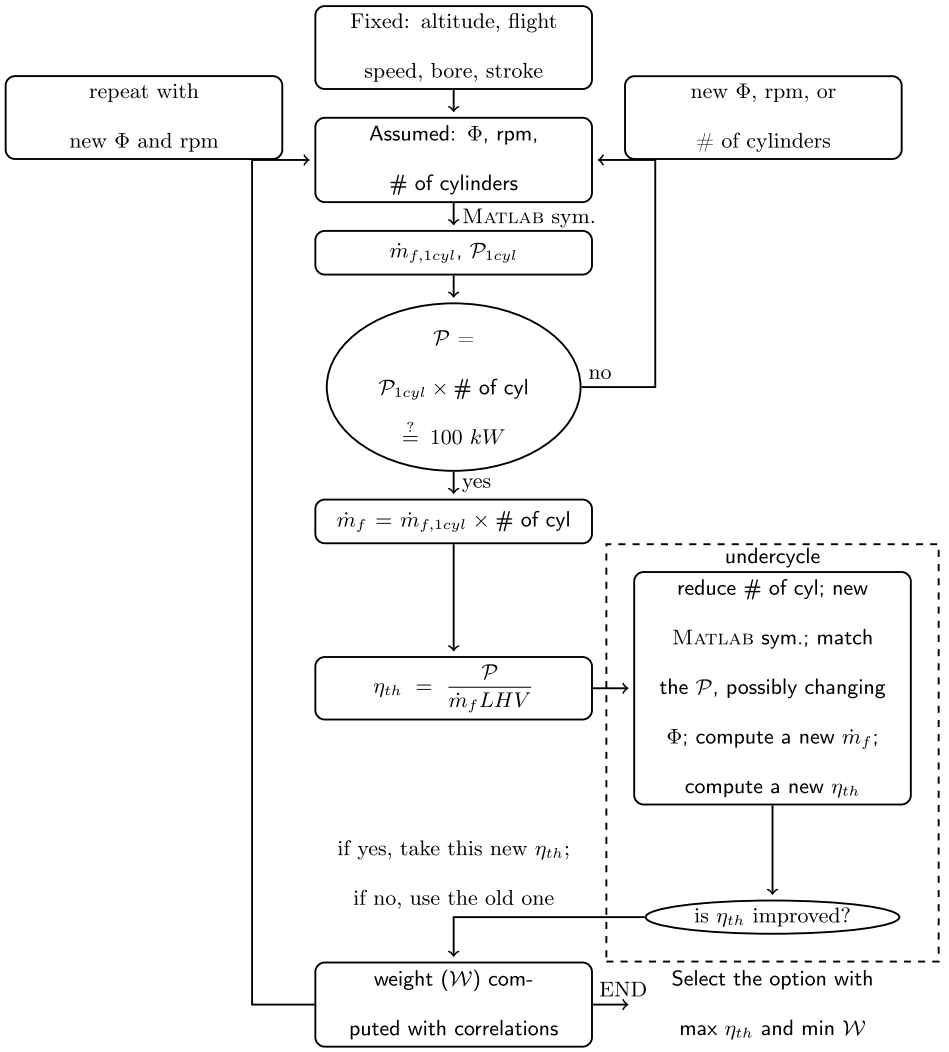

Fig. 3 Optimization process for IC engine.

and the engine rotation frequency must remain within reasonable limits for these applications (i.e., $\Phi = 0.8$–1.5 and rotation frequency of 1200–500 rpm). The optimization scheme is reported in Fig. 3.

Here is an example of the optimization process. Consider the four-stroke spark ignition engine; assume a flight altitude ($z = 10{,}000$). The cruise flight Mach number is 0.4. For the IC engines in Figs. 4 and 5, the cylinder geometry (bore = 8 cm, stroke = 9 cm) is kept constant with altitude and power. For a certain rotation frequency and equivalence ratio, a power is obtained from the code; this is the power obtained from one cylinder. This power must be multiplied for a hypothetical number

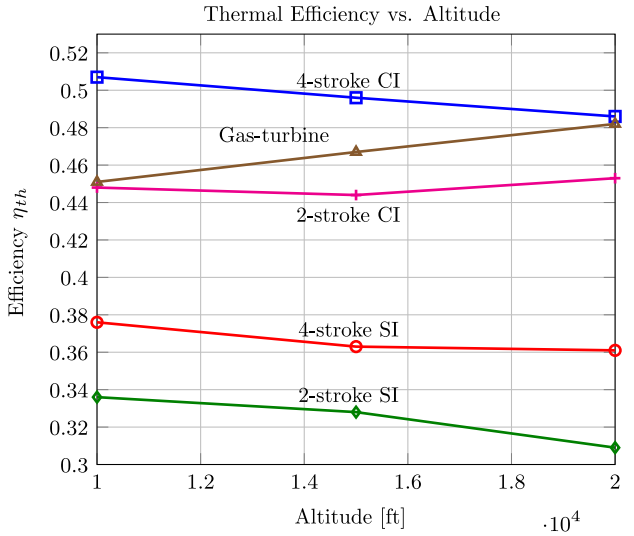

Fig. 4 Thermal efficiency of the five engines modeled by the Matlab codes as function of flight altitude; power: 150 kW.

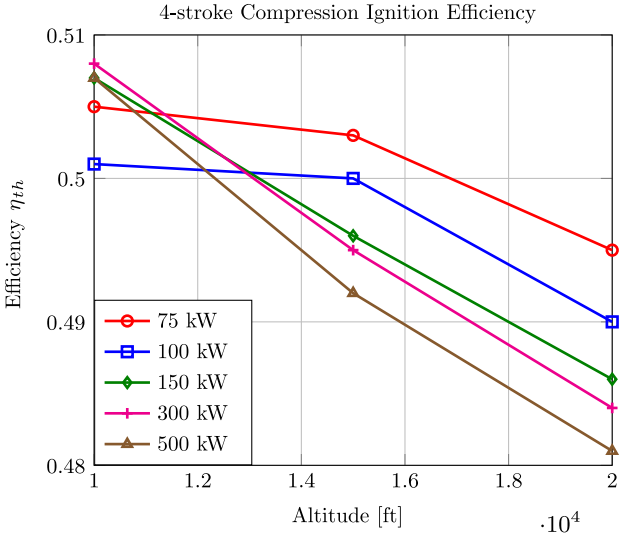

Fig. 5 Four-stroke diesel engine efficiency as function of flight altitude; power: 75–500 kW.

of cylinders to obtain the target power of the whole engine, say 125 kW. Few attempts are needed to obtain exactly 125 kW. Some finer adjustments of rotation frequency and equivalence ratio can be done here as well as the number of cylinders. The number of cylinders increases from four to six for powers higher than 100 kW to obtain better efficiencies. Once the power target is matched (within a fraction of a kilowatt), the thermal efficiency of the engine can be computed by

$$\eta_{th} = \frac{\mathcal{P}}{\dot{m}_f \mathrm{LHV}} \tag{1}$$

where P is the total power delivered from the engine (125 kW), and $\dot{m}_f$ is the sum of the fuel consumption of every cylinder. The weight of this configuration is evaluated by means of a correlation in the form $W = a + bP^c$, optimized with the coefficients in Table 4.

At this point, bore, stroke, and flight altitude are maintained constant, whereas rotation frequency and equivalence ratio are modified. With these variations, a different efficiency is obtained, although the power still matches the target. The turbocharging option for altitude compensation allows a limit for the efficiency depletion. Figures 4–6 show the result of this optimization process, presenting the engines with the highest efficiency only.

Figure 5 shows that a reciprocating engine loses efficiency when altitude increases; this is due to the lower density of the air and the consequent poor cylinder filling. For this reason, turbocharging is used to compensate this detriment. Above a certain size limit, a smaller high-rotation-frequency engine is generally more efficient than a large low-rotation-frequency engine. Hence, there exists benefit from using multiple small-scale reciprocating engines.

The turbine engine of Fig. 6 has an opposite behavior. The turbine engine efficiency is higher when altitude increases; in fact, the higher the cycle temperature ratio is, the higher the thermal efficiency is. The lowest temperature of the cycle is the environmental temperature, which decreases with altitude.

Finally, Fig. 4 shows that diesel engines are more efficient than the spark-ignition engine, and the four-stroke option is more efficient than the two-stroke. Hence, the gas turbine and the four-stroke diesel engine are the main competitors from a thermal efficiency viewpoint. For this reason, the further discussion will be based on these two options only, with the others being discarded. Hereafter, only the results for 10,000 ft will be considered because the same considerations are valid for the other altitudes.

Two important questions are to be answered in this study. First, between the diesel engine and gas turbine, which is the best choice to accomplish a long mission? Second, which engine–propeller layout (number, connections, size) gives the best performance? The second question requires consideration of two different overlapping effects: the weight and efficiency gain obtained by the choice of an engine–propeller layout instead of another, and the thrust benefit comes from a better choice of propeller size and number. For this reason, these two effects are studied separately. In the first subsection to follow, only the engines are compared, regardless of propellers size and efficiency. In the second subsection, the propeller theory defines the gain in thrust obtained by a certain propeller design. A third subsection briefly describes the criteria to integrate the two effects.

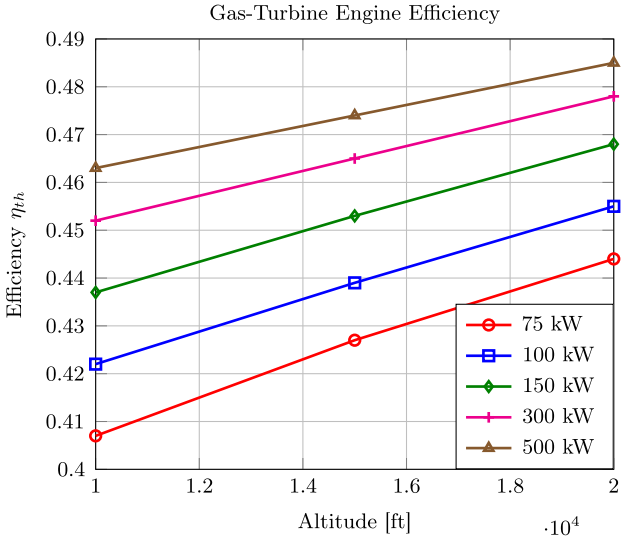

Fig. 6 Gas-turbine engine efficiency as function of flight altitude; power: 75–500 kW, OPR = 40.

A. Layout Selection

Four configurations are here compared (simplified sketches are shown in Fig. 7): 1) single engine, single propeller (configuration A); 2) single engine, belt transmission, three propellers (configuration B); 3) three engines, three propellers (configuration C); and 4) single engine, electric generator, two electric motors, three propellers (configuration D).

Data about the devices involved are reported in Table 5 [14–17]. Belt transmission is intended as the system made by two pulleys and a belt; the authors are aware that belt transmission is unlikely to be used for this scope, given the high torque required by aeronautical operations, but it is here reported as the lightest form of mechanical transmission, with respect to chain and gears transmission.

If the power output the engines must supply is fixed (e.g., 300 kW), it is evident that the best choice is a configuration with a direct engine–propeller connection, like configurations A and C. In fact, any other item added to the system (e.g., generator, belt transmission) would add weight and mechanical inefficiency; hence, a larger, heavier, and more fuel-consuming engine is necessary for configurations B and D. Moreover, engine weights do not scale linearly with power, as shown is Sec. II (i.e., three 100 kW engines are heavier than a single 300 kW). Hence, configuration A is the most efficient and lightest among the four.

Configuration A can be diesel-based or gas-turbine-based; the comparison over a 50 h mission with a generic intermittent auxiliary power profile is shown in Fig. 8. For flight missions shorter than 18 h, the turbine-based layout is the lightest because the dry weight of the machine is a great advantage. However, the lower fuel consumption for the diesel engine makes this technology the best solution for longer missions, even accounting for the larger engine weight.

B. Propeller Efficiency

The blade theory shows that propeller efficiency increases with increasing diameter for a fixed thrust. However, centrifugal forces must be kept below structural limits. A tip speed approaching transonic and sonic regions can produce excessive noise, shock waves, and vibrations. Hence, these factors limit the propeller size and rotation frequency. A complete discussion can be found in [18,19]. On the other hand, for a given total thrust, use of multiple smaller propellers can give better overall propulsion efficiency, which is the motivation for distributed propulsion. Choosing between these two opposite trends is not straightforward. A key point is that the thermal efficiency of a gas-turbine engine increases with its cross-sectional size. Instead, it is common experience in automotive industry that, for a given shaft power, a smaller highly loaded diesel engine is more efficient than a larger one operated at lower rotation frequency. Another issue is that propeller efficiency varies by just a few percentage points when varying the diameter (typical numbers are 85–88%, obtained via experimental test and supported by computational fluid dynamics simulations [20]), whereas scaling up or down the engine size is much more significant in terms of percentage. The preceding factors are included in the following analysis.

C. Final Comparison

The four configurations are sized to the same input power; given the different transmission efficiency and propeller size and number, the output thrust is different. Configurations B and D could become competitive only if the propulsive efficiency gain given by the use of multiple propellers overcomes the weight and efficiency penalization due to electrical conversion of the generator, mechanical friction of belt transmission, and the additional weight of multiple propellers

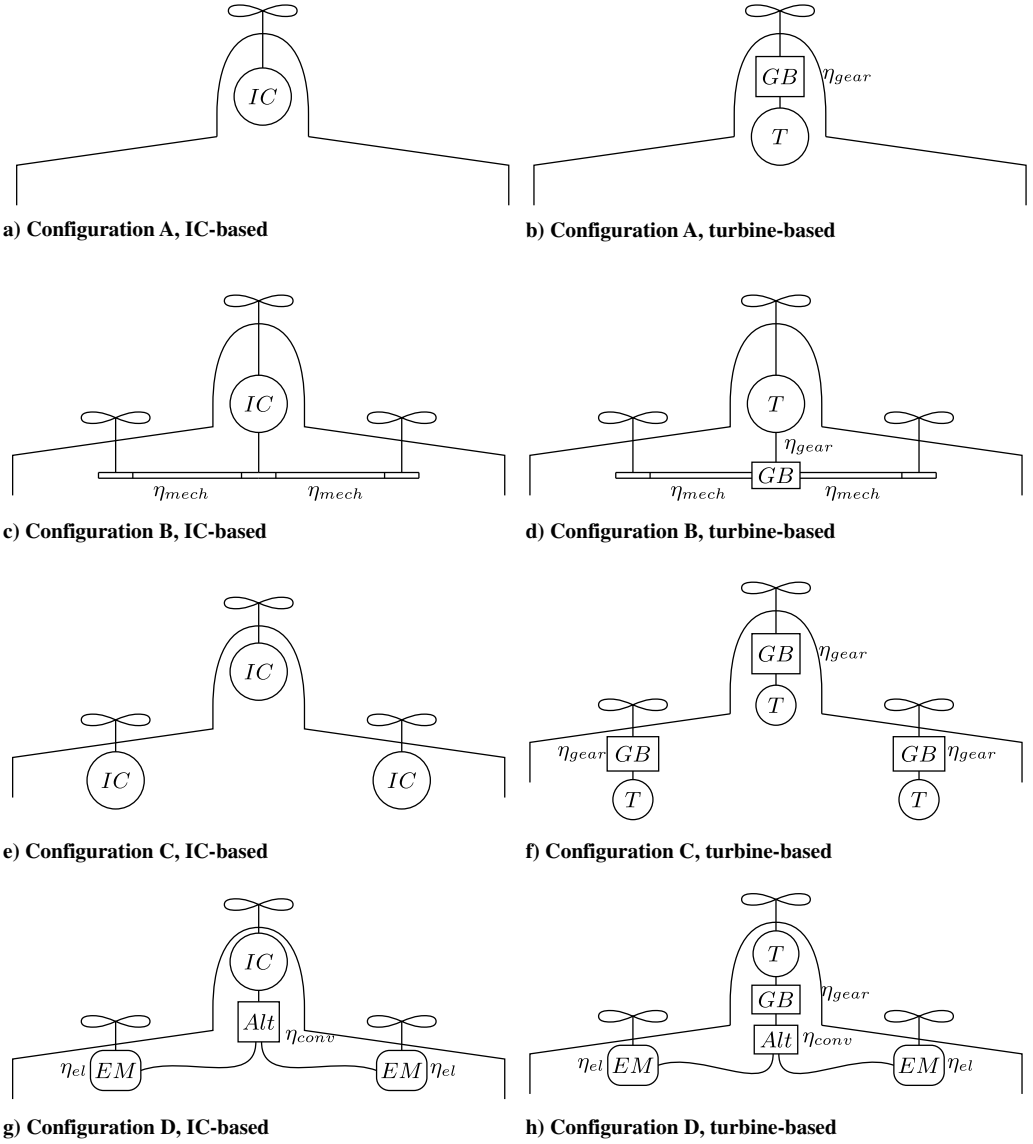

a) Configuration A, IC-based **b) Configuration A, turbine-based**

c) Configuration B, IC-based **d) Configuration B, turbine-based**

e) Configuration C, IC-based **f) Configuration C, turbine-based**

g) Configuration D, IC-based **h) Configuration D, turbine-based**

Fig. 7 Configurations considered for the analysis.

instead of one. Unfortunately, all these negative effects outweigh the thrust gain from multiple propellers at present. For this reason, the electric propulsion and the mechanical transmission are excluded from further consideration.

Table 5 Weight and efficiency of the devices involved in the configurations

Component	Weight, kg	η, %
Generator	10	80 [14]
Belt transmission	20	95 [15]
Electric motor	45	97 [16]
Gearbox	15	90 [17]

We now compare two new configurations: 1) single turbine, single (larger) propeller (configuration A); and 2) multiple diesel engines, multiple (smaller) propellers (configuration B).

Upon so doing, the turbine becomes as efficient as possible, with the larger propeller being lighter than three smaller propellers and not constituting a big disadvantage in terms of efficiency. The multiple-engine configuration experiences a lower propeller efficiency due to propeller size and pays the price of a higher dry weight of the entire assembly but also benefits from the use of more-efficient diesel engines.

These two layouts are then compared over two hypothetical mission profiles: an ideal constant-cruise-speed, constant-power mission, and a more-realistic mission involving higher thrust for takeoff and intermittent auxiliary power peaks (Fig. 9). The sizing procedure starts by fixing the power and the number of the diesel engines, the power of the turbine, and the propeller(s) geometry. By the use of the developed

Table 6 Performance data of the updated configurations

Name of configuration	D4	D3	D2	T1, $\pi = 40$	T1, $\pi = 60$
Number of propellers	4	3	2	1	1
Engines	4 diesels	3 diesels	2 diesels	1 turbine	1 turbine
Power, kW	125 each	169 each	260 each	594	594
Dry weight, kg	154 each	196 each	257 each	70	Around 80
Fuel consumption, l/h	24.02 each	33.29 each	52.92 each	134.16	123.33

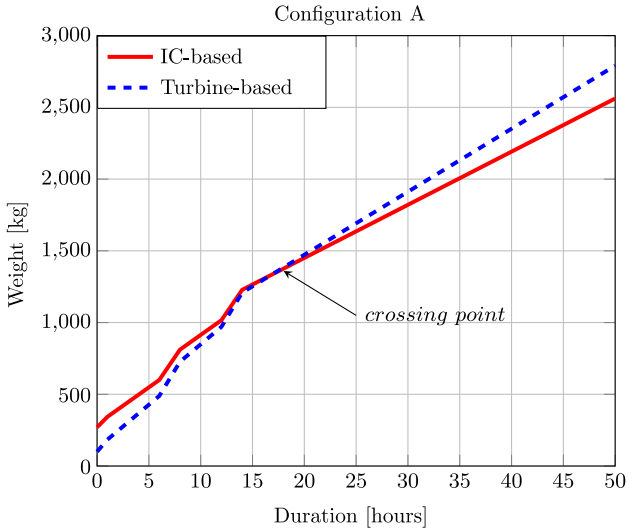

Fig. 8 Comparison between the turbine and diesel configurations A. Altitude = 10,000 ft.

Table 7 Performance data of the propellers selected

Number of propellers	4	3	2	1
Diameter, m	1.5	1.7	2.1	2.3
Rotation frequency, rpm	2500	2300	2000	1900
η_{prop}, %	89.5	89.0	88.5	88.0
J	2.10	2.02	1.88	1.81
C_P	0.252	0.234	0.190	0.289
C_T	0.201	0.201	0.200	0.198
Number of blades	3	3	3	3
Weight, kg	28	33	37	39
Input power, kW	125	169	260	535
Thrust, N	859	1146	1721	3587
Total power needed, kW	500	507	520	535
Total thrust, N	3436	3438	3442	3587

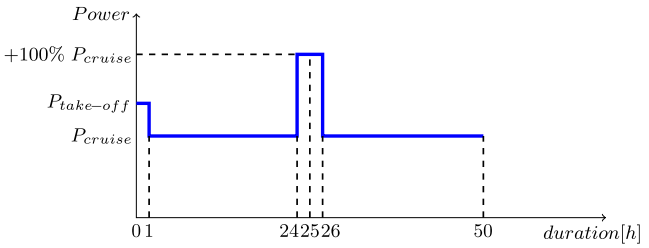

Fig. 9 Power requirement profile for 50 h mission.

Matlab codes, the engines' fuel consumption is computed. Considering a mission with up to 50 h duration, the fuel weight can be calculated. On the basis of the fuel weight and UAVs' typical design choices, the structural weight can be estimated following the procedure in [19] and briefly reported in Appendix C. Hence, the overall aircraft weight, lift, and drag are known. The thrust equals the drag if a constant-cruise mission is selected (Mach 0.4). Otherwise, a uniform, straight acceleration is considered during the takeoff phase. No matter how the thrust is computed, there is an important constraint: the chosen propeller assembly must be able to deliver that thrust to the aircraft. The thrust, power, geometry, and efficiency of the propellers are connected by

$$C_T = \frac{T}{\rho n^2 D^4} \qquad C_P = \frac{P}{\rho n^3 D^5} \qquad \eta_{\text{prop}} = \frac{TV}{P} \tag{2}$$

where ρ is the air density, n is the rotation frequency in revolutions per second, V is the flight speed, and D is the propeller diameter. These parameters cannot be chosen independently; helpful experimental diagrams are available in the literature. In this analysis, the diagrams reported in [21] are used. If T is not the desired one, two choices are possible. For small adjustments, it is sufficient to modify the propeller geometry; otherwise, it is necessary to vary the number and power of propellers and/or engines. If engine power is changed, new values of fuel consumption are produced with the Matlab codes, and an iterative process starts. Moreover, in the case in which auxiliary power is needed, a peak power of +100% with respect to cruise power is assumed for a short duration. In this scenario, a more powerful engine with larger fuel consumption must be considered for the non-constant-power mission. Hence, the aircraft is heavier at takeoff because of the need for more thrust (and power).

When convergence is reached, the aircraft engine and propellers are fully sized. Although the turbine configuration is single-engine, single-propeller, the diesel configuration can be designed to be two–two, three–three, and four–four of these elements. These variations of the "configuration A theme" are shown in Fig. 10. Data of their respective engines are shown in Table 6. The power reported there was considered as the cruise power at $M = 0.4$. Data about propellers designed after the optimization are reported in Table 7; they all have variable pitch, to provide constant rotational speed.

Propellers of Table 7 are taken from Roskam [22], which contains 43 pages of propeller charts, extracted from [21]. Concerning the variable-pitch mechanism, as discussed in other points of the paper (e.g., Sec. II), the presence or absence of a few gears (in the order of 10 kg) composing the mechanism would not make a significant difference in the computations because the overall weight of the drone at takeoff is two orders of magnitude higher.

Concerning the turbine technology, a compression ratio $\pi = 40$ represents the current state of the art [23,24]. A comparison with an advanced $\pi = 60$ is presented, showing the potential of investing in this technology; however, increasing π involves an increase in dimension and weight.

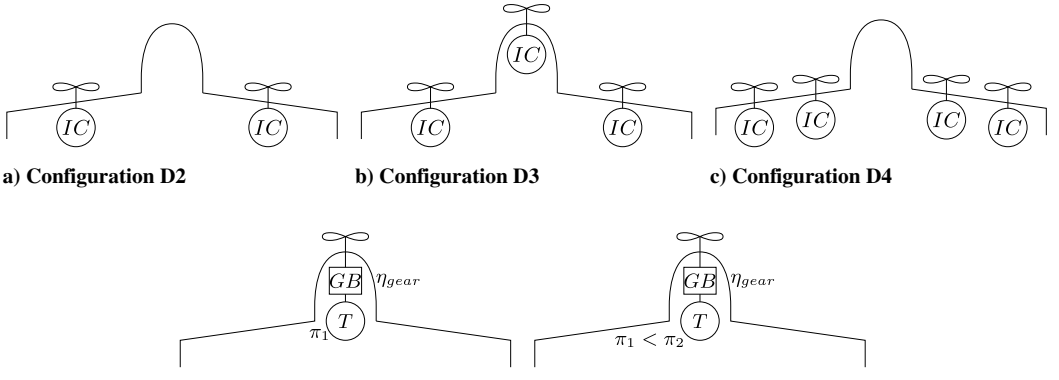

a) Configuration D2 **b) Configuration D3** **c) Configuration D4**

d) Configuration T1, $\pi = 40$ **e) Configuration T1, $\pi = 60$**

Fig. 10 Aircraft possible variations over configuration A layout.

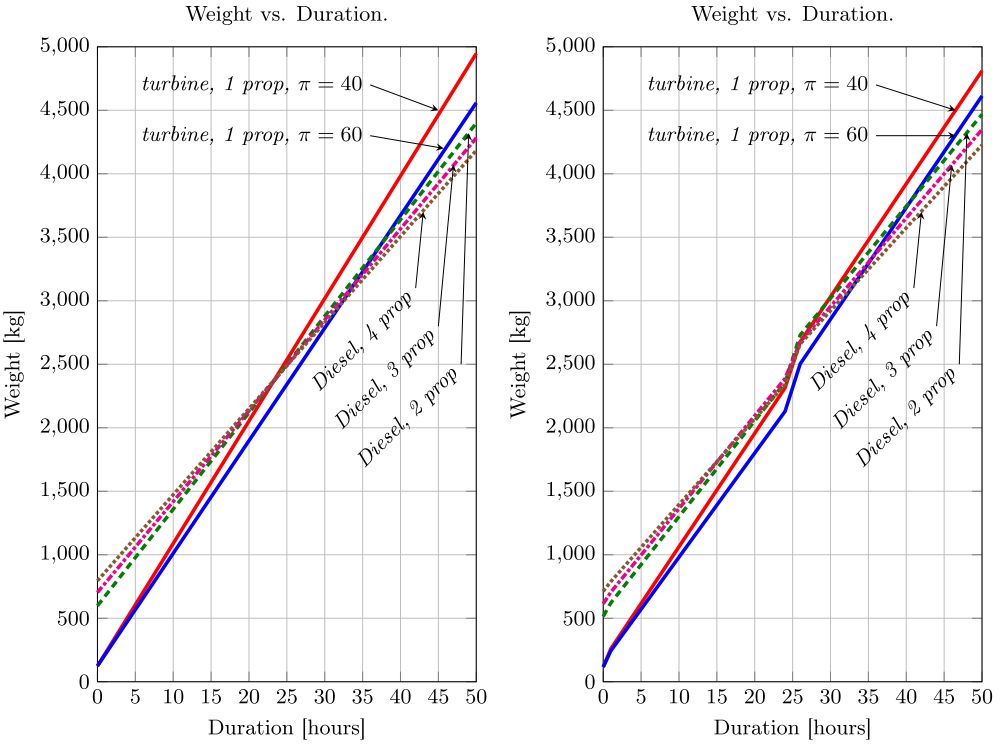

a) Constant cruise mission **b) Throttled mission**

Fig. 11 Comparison between different configurations. Altitude = 10,000 ft, flight Mach number 0.4.

The configurations obtained are tested over missions up to 50 h. Missions are of the simplest type, where the aircraft takes off, performs a straight path until half of the fuel is consumed, makes a 180 deg veer, and flies back to the starting point. No other changes of altitude or turns are considered. The results for the constant-cruise mission are shown in Fig. 11a. The weight reported in Fig. 11a is the takeoff gross weight, which decreases by the amount of fuel burned along the flight. For short durations, the gas-turbine configuration is lighter than the diesel configuration, with the four-engine, four-propeller configuration being the heaviest. At around 23 h flight, the diesel configuration surpasses the turbine configuration in performance, due to their higher efficiency. For longer missions, the four-engine, four-propeller configuration is the best configuration because of the lower fuel consumption of the smaller engines; a cutting-edge turbine with $\pi = 60$ would shift the crossing point upward to 31 h, due to the higher efficiency. Its dry weight is estimated to be approximately 10 kg larger than the $\pi = 40$ turbine.

Figure 11b takes into account also the additional thrust for takeoff and the auxiliary power phase, simulating a specific requirement to be accomplished at half mission. The crossing point shifts a little bit toward longer durations; the diesel configurations surpasses the $\pi = 40$ gas turbine at around 25 h of flight. With an increased compression ratio of 60, the turbine engine could extend its dominant range up to 34 h. This right shift of the crossing point (compared to the constant-cruise mission) is due to a different increase of fuel consumption between the configurations. The diesel engines, in particular, undergo a remarkable decrease in efficiency past the design point, when very high rotation frequencies are imposed. The gas turbine also shows a decrease in efficiency when shifting from its design point but less abrupt than in the IC engines. Hence, the increase in the curve slope is less severe, and the crossing point shifts toward longer durations.

IV. Conclusions

A thermal analysis has shown the advantages of replacing a small gas turbine with one or more turbocharged four-stroke diesel engines. The presence of the turbocharger for altitude compensation keeps the internal combustion (IC) engine at its best performance over a larger flight envelope. Increases in efficiency and decreases in fuel consumption can result. These advantages can translate to increases in range and/or flight duration, plus a reduction in fuel tank volume and weight. For the power range of about 300 kW, the use of multiple diesel engines coupled with the same number of propellers results in lower fuel weight for missions of durations beyond 23–25 h. Use of a future high-performance gas-turbine engine may push the breakeven point to 31–34 h.

Replacing a gas turbine with multiple diesel engines may present problems concerning the reliability of the system, as well as noise, vibrations, and size, which are very important requirements in a long-duration unmanned air vehicles. However, the use of reciprocating engines allows savings for purchase, maintenance, and use of a single fuel type as that for ground vehicles. Considerations on efficiency and weight have shown the nonfeasibility of using mechanical connections between one engine and multiple propellers or electric generators to drive electric motors. The availability of more-efficient electric generators and motors with advances in the development of superconductivity could cause reconsideration of the hybrid option in the future. Further improvements in IC engine efficiency and weight include different arrangements of the turbochargers; it is conceivable to save weight and volume if a single turbocharger could supply air to multiple engines simultaneously.

Appendix A: Internal Combustion Engines Modeling

A.1. Four-Stroke Compression Ignition (Diesel) Model

The thermodynamic cycle of the engine is subdivided into 720 deg (i.e., two complete revolutions of the crank). The index i is used to indicate the crank angle. The initial conditions at $i = 1$ are hard to be assessed because they are the consequence of the previous cycle. Hence, the initial conditions of the cycle are taken from an ideal Otto cycle, performed in advance. The cycle starts with the piston at bottom dead center (BDC), ready for

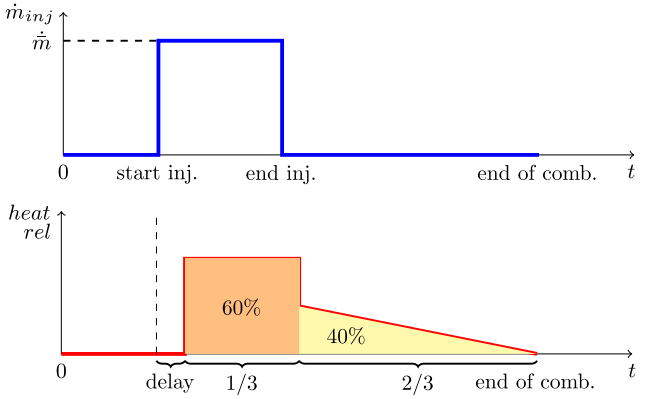

Fig. A1 Fuel injection and heat release profile.

compression stroke, with both the valves closed. The compression stroke is characterized by [25]

$$p_i = p_{i-1}\left(\frac{V_{i-1}}{V_i}\right)^{\gamma_c} \qquad T_i = T_{i-1}\left(\frac{V_{i-1}}{V_i}\right)^{\gamma_c - 1} \tag{A1}$$

where γ_c is the mixture specific heat ratio during compression stroke, constant and equal to 1.4; a corresponding $\gamma_e = 1.3$ for expansion is considered. The combustion process is modeled by a single zone in the cylinder, with uniform pressure and temperature. This simplifying assumption allows a reasonable computational time and accuracy, without focusing on the real (complex) mechanism of ignition. The fuel injection is assumed to happen in the liquid phase.

The first law of thermodynamics states $U = Q - W$, where U is the internal energy of the cylinder contents, W is the work, and Q is the heat. The heat is taken with positive sign when entering the control volume; the work is positive when it is done by the gases on the surroundings. The time derivative gives $\dot{U} = \dot{Q} - \dot{W}$; each term must be modeled. We assume a constant specific heat and use an average value over a temperature range:

1) $\dot{U} = \dot{m}c_v T + mc_v\dot{T} = \frac{R}{\gamma-1}(\dot{m}T + m\dot{T})$

2) $\dot{Q} = \dot{Q}_{\text{ch}} - \dot{Q}_{\text{ht}} + \dot{Q}_{\text{sens}}$

$\dot{Q} = \dot{m}_{\text{burn}}Q_{\text{LHV}} - hA(T - T_w) + \left(\sum_i \dot{m}_i h_i - \sum_j \dot{m}_j h_j\right)$

3) $\dot{W} = p\dot{V}$

where Q_{ch} is the energy released by combustion; Q_{ht} is the heat lost to the cylinder and piston walls; Q_{sens} is the sensible energy of those masses entering and leaving the volume (only fuel injection is considered; crevice losses and leakages are neglected); m is the cylinder mass at each time step; and Q_{LHV} is the fuel low heating value. Assembling the terms, we get the following equation:

$$\frac{R}{\gamma-1}(\dot{m}T + m\dot{T}) = \dot{m}_{\text{burn}}Q_{\text{LHV}} - hA(T - T_w) + \dot{m}_{\text{inj}}h_i - p\dot{V} \tag{A2}$$

By differentiating in time the perfect gas law and rearranging, we obtain

$$\dot{T} = \frac{\dot{p}V + p\dot{V} - \dot{m}_{\text{inj}}RT - m\dot{R}T}{mR} \tag{A3}$$

where T is simply given by the perfect gas law. By substituting Eq. (A3) into Eq. (A2) and rearranging,

$$\frac{R}{\gamma-1}\left[\dot{m}_{\text{inj}}T + \frac{1}{R}(\dot{p}V + p\dot{V} - \dot{m}_{\text{inj}}RT - m\dot{R}T)\right] = \dot{m}_{\text{burn}}Q_{\text{LHV}} - hA(T - T_w) + \dot{m}_{\text{inj}}h_i - p\dot{V}$$

$$\dot{p} = \frac{\gamma-1}{V}\left[\dot{m}_{\text{burn}}Q_{\text{LHV}} - hA\left(\frac{pV}{mR} - T_w\right) + \dot{m}_{\text{inj}}c_p T_f - p\dot{V}\right] - p\left(\frac{\dot{V}}{V} - \frac{\dot{R}}{R}\right) \tag{A4}$$

Equation (A4) is a differential equation in the form $\dot{p} = f(t, p)$. V and $\dot{V}$ are known from the cylinder geometry and rotation frequency. The term A in the preceding equation is the area subject to heat transfer. It is given by

$$A(\theta) = A_{\text{fix}} + A_{\text{var}}(\theta)\begin{cases} A_{\text{fix}} = \frac{\pi B^2}{2} + \frac{4V_c}{B} \\ A_{\text{var}}(\theta) = \frac{4(V(\theta) - V_c)}{B} \end{cases} \tag{A5}$$

where B is the cylinder bore, and V_c is the clearance volume. The presence of the term $\dot{R}$ increases the overall complexity of the problem. A possible solution is the shifting of the value of R in time with composition between two typical values: 289 J/(kg · K) for the exhaust gases, and 273 J/(kg · K) for the fresh charge. The rate of burning is modeled by the Wiebe function [Eq. (A6)] [25]:

$$R = x_b R_1 + (1 - x_b)R_2 \qquad \dot{R} = \frac{\mathrm{d}R}{\mathrm{d}x_b}\frac{\mathrm{d}x_b}{\mathrm{d}\theta}\frac{\mathrm{d}\theta}{\mathrm{d}t}$$

$$x_b(\theta) = 1 - \exp\left[-c\left(\frac{\theta - \theta_0}{\Delta\theta}\right)^{r+1}\right]$$

$$\frac{\mathrm{d}x_b}{\mathrm{d}\theta} = \frac{c(r+1)}{\Delta\theta}\left(\frac{\theta - \theta_0}{\Delta\theta}\right)^r \exp\left[-c\left(\frac{\theta - \theta_0}{\Delta\theta}\right)^{r+1}\right]$$

$$\dot{R} = (R_1 - R_2)\omega\frac{c(r+1)}{\Delta\theta}\left(\frac{\theta - \theta_0}{\Delta\theta}\right)^r \exp\left[-c\left(\frac{\theta - \theta_0}{\Delta\theta}\right)^{r+1}\right] \tag{A6}$$

According to [25], actual mass fraction curves have been fitted with $c = 5$ and $r = 2$. The characteristic shape of fuel injection $\dot{m}_{\text{inj}}$ and the fuel burning rate $\dot{m}_{\text{burn}}$ must now be modeled. The inlet fuel mass flow rate is given by the fuel flow through a nozzle:

$$\dot{m}_{\text{inj}} = C_d A_{\text{inj}}\sqrt{2\rho_f \Delta p}$$

$$m_{\text{inj}} = C_d A_{\text{inj}}\sqrt{2\rho_f \Delta p}\frac{\Delta\theta}{6\text{rpm}}$$

where A_{inj} is the nozzle area, ρ_f is the fuel density, Δp is the pressure drop across the injector, C_d is the discharge coefficient, and $\Delta\theta$ is the length of injection (in degrees). C_d, A_{inj}, ρ_f, and $\Delta\theta$ are fixed, whereas m_{inj} is an input parameter. It follows that $\Delta p(t)$ can be obtained by the second equation and substituted into the first. The magnitude of fuel mass flow rate is then known.

The ignition delay in a diesel engine is defined as the time (or crank angle) interval between the start of ignition and the establishment of the flame. Heywood [25] indicates that typical ignition delays lie between 5 and 9 deg. The real injection profile is available only from experimental data; in this analysis, a step function is assumed to approximate the injection rate. See Fig. A1.

The approximate heat release profile is modeled by two blocks: typically the 60% of the fuel is burned within the first third of combustion duration; then the rest is consumed linearly until there is no fuel to sustain the combustion [25].

The Annand correlation [26] is used to model the heat transfer coefficient h:

$$\left(\frac{hB}{k}\right) = a\left(\frac{\rho\bar{S}_p B}{\mu}\right)^b$$

where $\bar{S}_p$ is the mean piston speed, B is the piston bore, and k is the wall thermal conductivity.

Cylinder gases then follow a polytropic expansion until the exhaust valve is opened, some degrees before bottom dead center (BDC). When the exhaust valve opens, the cylinder pressure is above the exhaust manifold pressure, and a blowdown process occurs. A displacement of gas from the cylinder follows the blowdown process as the piston moves from BDC to top dead center. This process is modeled as follows. For subcritical flow, the mass flow rate through the valve is

$$\dot{m} = \frac{C_D A_T p_0}{\sqrt{RT_0}} \left(\frac{p_T}{p_0}\right)^{1/\gamma} \left\{\frac{2\gamma}{\gamma - 1}\left[1 - \left(\frac{p_T}{p_0}\right)^{(\gamma-1)/\gamma}\right]\right\}^{1/2} \tag{A7}$$

whereas for a choked flow, a similar equation is used:

$$\dot{m} = \frac{C_D A_T p_0}{\sqrt{RT_0}} \gamma^{1/2} \left(\frac{2}{\gamma + 1}\right)^{\gamma + 1/2(\gamma-1)} \tag{A8}$$

The mass flow rate $\dot{m}(i)$ depends on cylinder pressure $p_0(i)$; see Eqs. (A7) and (A8). However, the cylinder pressure depends on the mass contained in the volume (perfect gas law), which in turn depends on the mass flow entering and exiting the volume:

$$p_0(i) = \frac{m(i)}{V(i)} R\bar{T}(i) = \frac{m(i-1) + \left[\dot{m}_{\text{in}}(i) - \dot{m}_{\text{out}}(i)\right]\Delta t}{V(i)} R\bar{T}(i) \tag{A9}$$

where i indicates the crank angle, $\bar{T}$ is the average temperature between the cylinder and the manifold gases, and Δt is the time step of the computation. For this reason, an iterative process is needed; $p_0(i-1)$ is used to compute $\dot{m}(i)$ with Eqs. (A7) and (A8), and this value is used in Eq. (A9) to find a new value of pressure. The cycle is repeated until convergence.

The intake pressure is higher than the cylinder pressure, and fresh charge enters. The intake valve is kept open far after BDC, to enhance the loading of the cylinder; in fact, for turbocharged engines during the first degrees of compression, the pressure in the cylinder is lower than the manifold pressure. At the beginning of the new compression stroke, the cylinder state is described by p, T, and m, which are likely to be different than those at the same crank angle computed before. At this point, it is possible to perform a new cycle starting from the new values. The convergence is reached when the thermodynamic properties at the end of the intake process match the starting ones of the previous iteration under a certain tolerance. Convergence is generally obtained in 2–3 iterations. Although this iterative procedure is required to "close" the loop in a p–V diagram, the real behavior of a reciprocating engine is fully unsteady, and properties vary from one cycle to the other.

Figure A2 shows a comparison between the four-stroke compression–ignition model performed on MATLAB and the existing Centurion 2.0 produced by Thielert AG. It is a 155 hp, four in-line cylinders, liquid-cooled turbocharged diesel engine. Some of its specifications are reported in Table A1. The simulation is performed at 15,000 ft (4600 m).

The numerical model shows a good match with the engine data sheet, for the whole rotation frequency range considered. Unfortunately, the literature data do not show the whole engine rotation frequency spectrum; however, the numerical trend forecasts a maximum power around 2400 rpm in agreement with the real curve projection.

A.2. Four-Stroke Spark Ignition Model

The main difference with the diesel model is the combustion process. At a certain point of the compression stroke, the spark plug ignites the cylinder contents, which is a mixture of air and fuel. The other (minor) difference is that the mass in the cylinder is constant during compression, combustion, and expansion, and premixed charge is drawn during the intake phase.

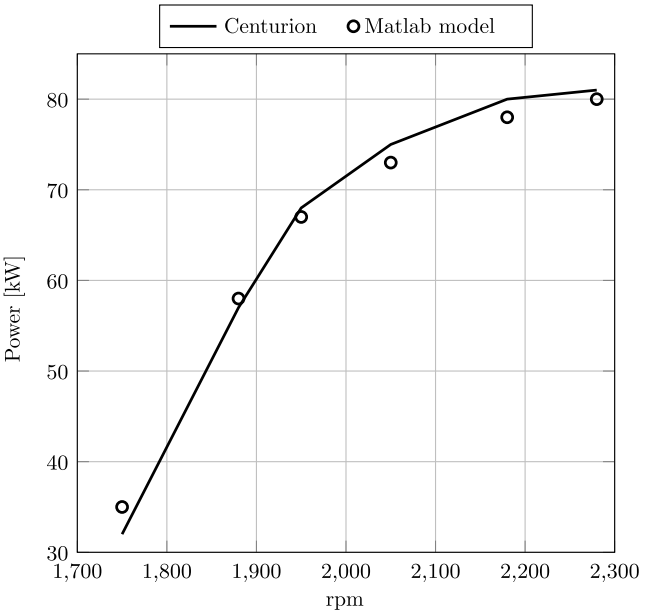

Fig. A2 Shaft power vs rotation frequency for the four-stroke turbocharged diesel model and the Thielert Centurion 2.0. Altitude = 4600 m; turbocharging compression ratio $\pi_c = 1.8$ at 1750 rpm, $\pi_c = 3$ at 2300 rpm.

The combustion model involves a two-zone volume: the burning zone and the unburned zone. By hypothesis, the two zones do not mix; however, their volumes V_b, V_u and temperatures T_b, T_u can change. Finally, the two zones are assumed to have the same pressure, which changes in time. Again, the first law of thermodynamics and its time derivative state

$$U = Q - W \qquad \dot{U} = \dot{Q} - \dot{W} \tag{A10}$$

1) $\dot{U} = \dot{m}_u c_{vu} T_u + m_u c_{vu} \dot{T}_u + \dot{m}_b c_{vb} T_b + m_b c_{vb} \dot{T}_b$

$$\dot{U} = m\left[-\frac{\mathrm{d}x_b}{\mathrm{d}\theta}\omega c_{vu} T_u + (1 - x_b) c_{vu} \dot{T}_u + \frac{\mathrm{d}x_b}{\mathrm{d}\theta}\omega c_{vb} T_b + x_b c_{vb} \dot{T}_b\right]$$

2) $\dot{Q} = \dot{Q}_{\text{ch}} - \dot{Q}_{\text{ht}}$

$$\dot{Q} = m_f \frac{\mathrm{d}x_b}{\mathrm{d}\theta}\omega Q_{\text{LHV}} - hA(T_b - T_w)$$

3) $\dot{W} = p\omega \dfrac{\mathrm{d}V}{\mathrm{d}\theta}$

where the mass fraction burned, x_b, is given by the Wiebe formula. By definition, $m_b = x_b m$ and $m_u = (1 - x_b)m$. To proceed further, models for T_b and T_u are required:

$$pv_b = R_b T_b; \qquad pv_u = R_u T_u$$

These equations give, after some manipulation,

$$\frac{pV}{m} = x_b R_b T_b + (1 - x_b) R_u T_u \tag{A11}$$

Table A1 Thielert AG Centurion 2.0 and Matlab model engine specifications

Specifications	Centurion 2.0	Model
Cylinder diameter, mm	83	83
Piston stroke, mm	92	92
Compression	18:1	18:1
Weight (correlation), kg	134	169

Table A2 Rotax 914UL and Matlab model engine specifications

Specifications	Rotax 914UL	Model
Cylinder diameter, mm	79.5	79.5
Piston stroke, mm	61	61
Compression	9:1	9:1
Weight (correlation), kg	64	115

An isentropic compression from an initial uniform state can be assumed for the unburned gas:

$$T_u = T_0\left(\frac{p}{p_0}\right)^{(\gamma-1)/\gamma} \tag{A12}$$

Substituting Eq. (A12) into Eq. (A11), we obtain

$$T_b = \frac{1}{mR_b x_b}[pV + (x_b - 1)mR_u T_u] \tag{A13}$$

Equations (A12) and (A13) and their time derivatives [Eqs. (A14) and (A15)] are all needed to close the problem:

$$\dot{T}_u = T_0\left(\frac{\gamma-1}{\gamma}\right)\left(\frac{p}{p_0}\right)^{(-1/\gamma)}\frac{\dot{p}}{p_0} \tag{A14}$$

$$\dot{T}_b = \frac{-\omega(\mathrm{d}x_b/\mathrm{d}\theta)}{mR_b x_b^2}[pV + (x_b - 1)mR_u T_u] + \frac{1}{mR_b x_b}\left[V\dot{p} + \frac{\mathrm{d}V}{\mathrm{d}\theta}\omega p + \frac{\mathrm{d}x_b}{\mathrm{d}\theta}\omega mR_u T_u + (x_b - 1)mR_u\dot{T}_u\right] \tag{A15}$$

Substituting Eqs. (A12–A15) into Eq. (A10), a differential equation in the form $\dot{p} = f(t, p)$ is obtained.

The thermodynamic cycle of a four-stroke spark-ignition engine has been investigated. The code has been compared with an existing engine, to test its accuracy. The engine chosen for the analysis is the Rotax 914UL, whose specifications are reported in Table A2. For this comparison, the power curve (Fig. A3) is available.

The comparison is made at 2000 m because this is the altitude that the Rotax 914UL reports in its data sheet. The simulated power curve agrees with the real curve; the classical concave shape is obtained, with the maximum around 6000 rpm.

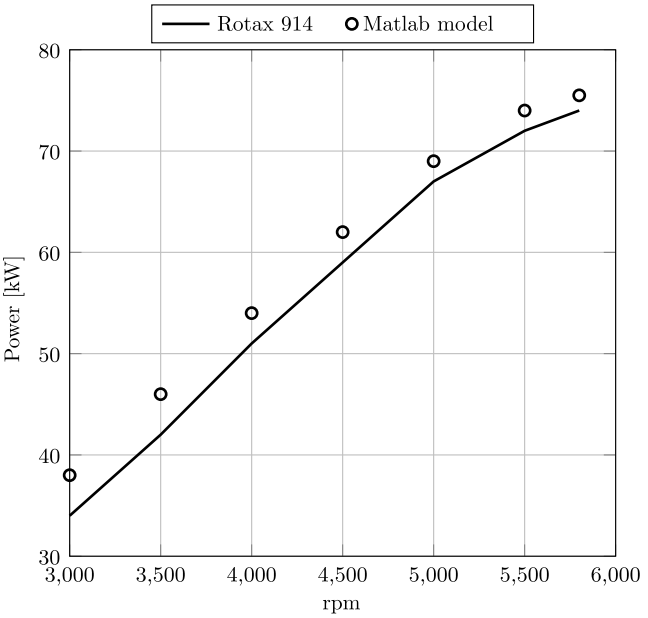

Fig. A3 Shaft power vs rotation frequency for the four-stroke turbocharged spark-ignition model and the Rotax 914. Altitude = 2000 m.

A.3. Two-Stroke Compression Ignition and Spark Ignition Models

The Matlab code developed here is inspired by the work of Sookdeo [27], though several major changes are done. The work of Sookdeo aims to model an extremely small and fast rotating CI engine, whereas we are interested in traditional dimensions and rotation frequency; for this reason, the engine geometry is rearranged. Moreover, the combustion model present in Sookdeo's work is oversimplified and fitted to experimental data performed by himself; it is necessary to implement a new combustion model (substantially equal to those previously explained), which has a general validity. Finally, a new heat transfer model was included.

The piston divides two environments: the volume contained between the piston and the cylinder walls, and the so-called crankcase (Fig. A4). The Matlab code evaluates five thermodynamic properties for each environment: cylinder pressure, mass of gases in cylinder, enthalpy, temperature, and entropy. For each one of these unknowns, an equation is required:

$$\begin{cases} pV = mRT \\ m = m_0 + m_{\text{in}} - m_{\text{out}} \\ Q = Q_0 + Q_{\text{in}} - Q_{\text{out}} \\ Q = mc_v T \\ Q = TdS \end{cases} \rightarrow \begin{cases} \dfrac{\mathrm{d}p}{\mathrm{d}\theta}V + p\dfrac{\mathrm{d}V}{\mathrm{d}\theta} = \dfrac{\mathrm{d}m}{\mathrm{d}\theta}RT + mR\dfrac{\mathrm{d}T}{\mathrm{d}\theta} & \text{Equation of state} \\ \dfrac{\mathrm{d}m}{\mathrm{d}\theta} = \dfrac{\mathrm{d}m_{\text{in}}}{\mathrm{d}\theta} - \dfrac{\mathrm{d}m_{\text{out}}}{\mathrm{d}\theta} & \text{Mass conservation} \\ \dfrac{\mathrm{d}Q}{\mathrm{d}\theta} = \dfrac{\mathrm{d}Q_{\text{in}}}{\mathrm{d}\theta} - \dfrac{\mathrm{d}Q_{\text{out}}}{\mathrm{d}\theta} & \text{Energy conservation} \\ \dfrac{\mathrm{d}Q}{\mathrm{d}\theta} = \dfrac{\mathrm{d}m}{\mathrm{d}\theta}c_v T + mc_v\dfrac{\mathrm{d}T}{\mathrm{d}\theta} & \text{First law of thermodynamics} \\ \dfrac{\mathrm{d}Q}{\mathrm{d}\theta} = \dfrac{\mathrm{d}T}{\mathrm{d}\theta}S + T\dfrac{\mathrm{d}S}{\mathrm{d}\theta} & \text{Second law of thermodynamics} \end{cases} \tag{A16}$$

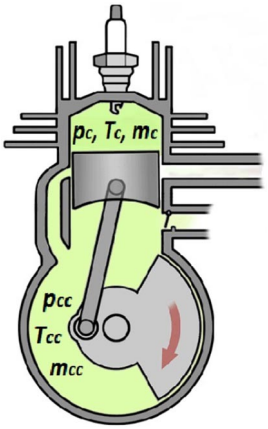

Fig. A4 Environments constituting a two-stroke engine cylinder.

Equations (A16) represent a system of five equations with five unknowns. Including the other set of five equations for the second environment, a 10×10 system in the form $M(t,x)\dot{x} = f(t,x)$ is obtained. In this case, the problem is made by the following linear system:

$$\begin{bmatrix} V_c & -RT_c & 0 & -m_cR & 0 & & & & & \\ 0 & 1 & 0 & 0 & 0 & & & & & \\ 0 & 0 & 1 & 0 & 0 & & & [\varnothing] & & \\ 0 & -c_vT_c & 1 & -m_cc_v & 0 & & & & & \\ 0 & 0 & 1 & -S_c & -T_c & & & & & \\ & & & & & V_{cc} & -RT_{cc} & 0 & -m_{cc}R & 0 \\ & & & & & 0 & 1 & 0 & 0 & 0 \\ & & [\varnothing] & & & 0 & 0 & 1 & 0 & 0 \\ & & & & & 0 & -c_vT_{cc} & 1 & -m_{cc}c_v & 0 \\ & & & & & 0 & 0 & 1 & -S_{cc} & -T_{cc} \end{bmatrix}$$

$$\times \frac{\mathrm{d}}{\mathrm{d}\theta} \begin{Bmatrix} p_c \\ m_c \\ Q_c \\ T_c \\ S_c \\ p_{cc} \\ m_{cc} \\ Q_{cc} \\ T_{cc} \\ S_{cc} \end{Bmatrix} = \frac{1}{\omega} \begin{Bmatrix} -\omega p_c \frac{\mathrm{d}V}{\mathrm{d}\theta} \\ \dot{m}_{cc} - \dot{m}_{\mathrm{out}} \\ \dot{Q}_{\mathrm{in}} - \dot{Q}_{\mathrm{out}} \\ 0 \\ 0 \\ -\omega p_{cc} \frac{\mathrm{d}V}{\mathrm{d}\theta} \\ \dot{m}_{\mathrm{in}} - \dot{m}_{cc} \\ \dot{Q}_{\mathrm{in}} - \dot{Q}_{\mathrm{out}} \\ 0 \\ 0 \end{Bmatrix} \tag{A17}$$

with initial conditions

$$x_0 = \begin{Bmatrix} p_c^0 & m_c^0 & 0 & T_c^0 & 0 & p_{cc}^0 & m_{cc}^0 & 0 & T_{cc}^0 & 0 \end{Bmatrix}^T \tag{A18}$$

Initial pressure and temperature of the cylinder are assumed as $p_c^0 = 1.4 p_{\mathrm{amb}}$ and $T_c^0 = T_{\mathrm{amb}} 1.4^{(\gamma-1)/\gamma}$. Further iterations will overwrite these values with the effective ones computed from the cycle. p_{cc}^0 and T_{cc}^0 are set equal to the conditions in the intake manifold: $p_{cc}^0 = \pi_c p_{\mathrm{amb}}$ and $T_c^0 = T_{\mathrm{amb}} \pi_c^{(\gamma-1)/\gamma}$. Finally, initial masses m_c^0 and m_{cc}^0 are computed with the perfect gas law:

$$CI: \begin{cases} m_c^0 = m_{\mathrm{air}} = \dfrac{p_c^0 V_c^0}{RT_c^0} \\ m_{cc}^0 = \dfrac{p_{cc}^0 V_{cc}^0}{RT_{cc}^0} \end{cases}$$

$$SI: \begin{cases} m_c^0 = m_{\mathrm{air}} + m_f = (1 + \alpha_{\mathrm{st}}\Phi) \dfrac{p_c^0 V_c^0}{RT_c^0} \\ m_{cc}^0 = (1 + \alpha_{\mathrm{st}}\Phi) \dfrac{p_{cc}^0 V_{cc}^0}{RT_{cc}^0} \end{cases} \tag{A19}$$

Now, α is defined as the fuel-to-air ratio. The system of differential equations is integrated along 360 deg with ode45 solver, obtaining the vector x at every crank angle. The Matlab solver ode45 is based on an explicit Runge–Kutta formula, the fourth-order-accurate Dormand–Prince method. It is a single-step solver, meaning that, in computing the solution at time t, it needs only the solution at the immediately preceding time point $t - 1$ [28]. The time step used for the four reciprocating engine models is varied between one crank angle up to 1/16 of a crank angle. Aside from a moderate increase in computational time, no significant change in the results occurs.

Appendix B: Gas-Turbine Engine Model

In this section, a cycle analysis of the gas turbine engine is performed to assess its efficiency for certain design choices, such as the compressor overall pressure ratio (OPR). The ideal thermodynamic cycle for the gas-turbine engine is the Brayton cycle (Fig. B1). In this study, the compressor OPR $\pi_c = p_{03}/p_{02}$ and the turbine inlet total temperature T_{04} are design choices. The OPR is evenly distributed throughout the compressor stages. The following parameters are also introduced as input in the code: flow coefficient $\Phi = V_x/U$, stage loading coefficient $\Psi = \Delta h_l/U^2$, degree of reaction $R = \Delta h_r/\Delta h_{\mathrm{stage}}$, and solidity $\sigma = c/s$. Other parameters are chosen as shown in Table B1.

Let the freestream be designated as station a at ambient pressure p_a and Mach number M; the inlet/diffuser reduces the flow to a low-speed flow before the compressor inlet; at station 02, $p_{02} = p_{01}/\pi_d$. The flow is further compressed to reach a total pressure $p_{03} = \pi_c p_{02}$ before it goes into the combustor; here, heat $\dot{Q}_b$ is added to increase the flow temperature up to T_{04}. A small loss in total pressure during combustion is found as $p_{04} = \pi_b p_{03}$. The high-temperature and high-pressure gas finally expands through the turbine to ambient pressure $p_{05} = p_a$.

The value of OPR is of extreme importance because it influences the thermal efficiency of the cycle. Typical gas-turbine engines have an OPR upper-limited to 40, like the CFM International Leading Edge Aviation Propulsion engine [24]. For this reason, $\pi_c = 40$ is taken as a reference value for current technology, and this value is used throughout the results. As a comparison, the results obtained by using $\pi_c = 60$ will be also plotted for showing the consequences of investing into this technology. The following assumptions have been made: 1) no air bleeding from the compressor, 2) complete expansion

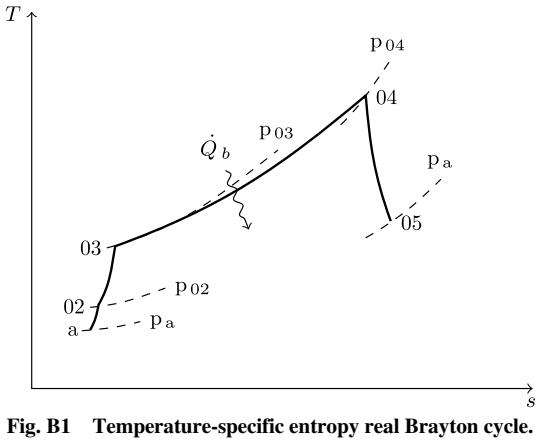

Fig. B1 Temperature-specific entropy real Brayton cycle.

Table B1 Input parameters of the gas-turbine numerical code

Parameter	Value
Altitude z	10,000 ft
Flight Mach number M_0	0.4
Diffuser pressure ratio π_d	0.98
Combustion chamber pressure ratio π_b	0.98
Combustion efficiency η_b	0.99
Mechanical efficiency η_m	0.98
Turbine inlet temperature T_{04}	1670 K

($p_5 = p_a$), 3) calorically perfect gas, and 4) part of the turbine power is used to drive the compressor, part to drive the propeller.

Typically, a compressor and turbine have many stages with approximately equal pressure ratios for each stage. However, Frisch [1] showed that, as the size of the compressor is reduced, the compression efficiency through each stage decreases due to increased losses [1]. There are four major loss mechanisms for compressors: blade surface boundary-layer dissipation, wake mixing dissipation, end-wall boundary-layer dissipation, and tip clearance flow dissipation. The efficiency loss related to these mechanisms has been described in [29–32]. As the size of a compressor decreases, the boundary-layer and mixing losses increase due to decreased Reynolds number. The relative tip clearance increases significantly as the compressor blade is shortened because the absolute tip gap cannot decrease proportionally due to manufacturing limitations, leading to substantially increased tip clearance loss. These losses strongly penalize the use of gas-turbine engines at very low power levels.

Accounting for all these forms of losses, it is possible to compute the adiabatic efficiency for the compressor. The adiabatic efficiency for the compressor and turbine are defined as

$$\eta_c = \frac{\pi_c^{((\gamma-1)/\gamma)} - 1}{\tau_c - 1} \tag{B1}$$

$$\eta_t = \frac{\tau_t - 1}{\pi_t^{((\gamma-1)/\gamma)} - 1} \tag{B2}$$

where $\tau_c = T_{03}/T_{02}$, $\tau_t = T_{04}/T_{05}$, and $\pi_t = p_{04}/p_{05}$. The following steps are used in the cycle calculations.

1) Inlet and diffuser section (a-02):

$$T_{02} = T_a\left(1 + \frac{\gamma - 1}{2}M^2\right) \tag{B3}$$

$$p_{02} = \pi_d p_a\left[1 + \eta_d\left(\frac{T_{02}}{T_a} - 1\right)\right]^{\gamma/(\gamma-1)} \tag{B4}$$

where γ is the air specific heat ratio, M is the flight Mach number, and η_d is the adiabatic efficiency of the inlet and diffuser.

2) Compressor (02–03): The stagnation temperature ratio can then be calculated starting from the OPR $\pi_c = p_{03}/p_{02}$:

$$\tau_c = \frac{T_{03}}{T_{02}} = 1 + \frac{1}{\eta_c}\left(\pi_c^{((\gamma-1)/\gamma)e_c} - 1\right) \tag{B5}$$

where η_c is the adiabatic efficiency of the compressor. The power needed to drive the compressor is then

$$P_c = \eta_c \dot{m}_a c_p T_{02}(\tau_c - 1) \tag{B6}$$

where η_c is the compressor isentropic efficiency, and $\dot{m}_a$ is the air inlet mass flow rate.

3) Main burner (03–04): The air-to-fuel ratio $\alpha = m_a/m_f$ can be calculated by an energy balance at the combustor:

$$\eta_b Q_b \dot{m}_f T_m + \dot{m}_a c_p T_{03} = (\dot{m}_a + \dot{m}_f) c_p T_{04} \tag{B7}$$

$$\alpha = \frac{\eta_b Q_b T_m - c_p T_{04}}{c_p(T_{04} - T_{03})} \tag{B8}$$

where Q_b is the fuel low heating value, η_b is the combustion efficiency, and T_m is the average temperature between T_{03} and T_{04}. p_{04} can be determined as $p_{04} = \pi_b p_{03}$.

4) Total turbine power (04-a): Finally, the hot gases are expanded through the turbine to produce enough power to drive the compressor and other utilities:

$$P_t = \eta_t(\dot{m}_a + \dot{m}_f) c_p T_{04}\left[1 - \left(\frac{p_a}{p_{04}}\right)^{(\gamma-1)/\gamma}\right] \tag{B9}$$

where η_t is the turbine isentropic efficiency. The net shaft power output of the turbine is $P_s = P_t - P_c$. The overall thermal efficiency of the engine is then $\eta_{\text{th}} = P_s/\dot{m}_f Q_b$.

Previous works showed the benefits of burning extra fuel in the first stages of the turbine [33–35]. The so-called turbine-burner technology allows significant increases in specific thrust with only small increases in thrust-specific fuel consumption. Future studies might consider use of the turbine burner for the production of auxiliary power.

Appendix C: Preliminary Sizing of the Aircraft

To proceed further in the analysis, the weight of the fuel (W_{fuel}) needed to accomplish the mission should be known. Moreover, the weight of the engines (W_{engine}) can be computed by means of correlations. The overall weight of the aircraft at takeoff includes also the weight of the structure and the payload, which need to be modeled.

In his work, Raymer [19] suggests a procedure to estimate the "design takeoff gross weight", which is defined as the total weight of the aircraft as it begins the mission for which it was designed. Design takeoff gross weight can be divided into crew weight, payload (or passenger) weight, fuel weight, and empty weight. The empty weight includes the structure, engines, landing gear, fixed equipment, avionics, and anything else not considered a part of crew, payload, or fuel. Equation (C1) summarizes the takeoff weight buildup:

$$\mathcal{W}_0 = \mathcal{W}_{\text{crew}} + \mathcal{W}_{\text{payload}} + \mathcal{W}_{\text{fuel}} + \mathcal{W}_e \tag{C1}$$

Because a UAV is the target of this analysis, no crew is involved in the mission. The payload, not well defined yet, might be composed by electronic devices like cameras, avionics systems, or weapons. Depending on the mission, it can be considered as an external input. Hence, the only unknown is the empty weight W_e, which is a function of the total aircraft weight itself, W_0. To simplify calculations, the empty weight can be expressed as a fraction of the total takeoff weight:

$$\mathcal{W}_0 = \mathcal{W}_{\text{payload}} + \mathcal{W}_{\text{fuel}} + \left(\frac{\mathcal{W}_e}{\mathcal{W}_0}\right)\mathcal{W}_0 \tag{C2}$$

The empty-weight fraction W_e/W_0 can be estimated statistically from historical trends; data are shown in [19] and are fitted so that correlations are obtained. These fractions vary from about 0.3 and 0.7 and diminish with increasing total aircraft weight. This dependence can be expressed by the exponential equation (weights are expressed in pounds):

$$\frac{\mathcal{W}_e}{\mathcal{W}_0} = a\mathcal{W}_0^b \tag{C3}$$

where a and b are coefficients depending on aircraft mission and size. Note that the empty-weight fraction depends on $\mathcal{W}_0$. The exponent b is a small negative number, which indicates that the empty weight fraction decreases with increasing takeoff weight. For military

long-range aircraft, $a = 0.93$, $b = -0.07$. Equations (C2) and (C3) constitute a nonlinear system of two equations in the two unknowns $\mathcal{W}_0$ and $\mathcal{W}_e$, which can be solved numerically.

Once the takeoff gross weight is known, it is easy to compute the lift at takeoff, which can be approximated equal to the aircraft full weight: $L = \mathcal{W}_0$. The remaining unknown in the estimate of the thrust is L/D, or lift-to-drag ratio. L/D is highly dependent upon the wing span, shape, and airfoil shape distribution. In this preliminary design, these data are still unknown to the designer; existing literature data are one means around this difficulty. If we assume the reconnaissance drone target of this thesis to be similar in shape to (but bigger in size than) the General Atomics MQ-1 Predator, the same aspect ratio can be assumed: $\mathcal{AR}$ [3]. $\mathcal{AR}$=19 is defined as the wing span squared divided by the wing reference area. Raymer suggests to correct the aspect ratio with the total aircraft wetted area, forming a new parameter, the "wetted aspect ratio" (WAR) [19]:

$$\mathcal{AR} = \frac{b^2}{A_{\text{ref}}}$$

$$\text{WAR} = \frac{b^2}{A_{\text{wet}}} = \frac{\mathcal{AR}}{A_{\text{wet}}/A_{\text{ref}}}$$

where $A_{\text{wet}}/A_{\text{ref}}$ is the wetted-area ratio.

According to Raymer's work, we can assume for the present study that $A_{\text{wet}}/A_{\text{ref}} = 7$. Hence, WAR = 2.7. A scatter plot reporting L/D as function of WAR for many aircraft families is available. Because the MQ-1 Predator is a fixed-landing-gear prop aircraft, a WAR of 2.7 corresponds to a $L/D = 15$. Finally, because L is known, the drag and the corresponding thrust can be computed.

Acknowledgments

The authors were encouraged by the original suggestion from Kenneth M. Rosen (General Aero-Science Consultants, LLC) that the diesel engine could compete with the gas-turbine engine at lower power levels. Valuable insights about the application of reciprocating engines were provided by Roy Primus (GE Global Research) and Patrick Pierz (Insitu, Inc.). The first author would like to thank the Politecnico di Milano for supporting through its International Mobility Program his graduate research at the University of California, Irvine.

References

[1] Frisch, A. M., "Scaling Effects on the Performance and Efficiency of Gas Turbine Engines," M.S. Project Rept., Dept. of Mechanical and Aerospace Engineering, Univ. of California, Irvine, CA, 2014.

[2] Peck, M., "U.S. Air Force Seeks Ideas for De-Icing Reapers," *Aerospace America*, Vol. 54, No. 3, March 2016, p. 5.

[3] "USAF MQ-1B Fact Sheet," U.S. Air Force, Air Force Departmental Publishing Office (AFDPO), Sept. 2015, http://www.af.mil/AboutUs/FactSheets/Display/tabid/224/Article/104469/mq-1b-predator.aspx [retrieved 23 Sept. 2015].

[4] Stevenson, B., "Export-Licensed Predator Makes Maiden Flight," Flight Global, London, July 2014, https://www.flightglobal.com/news/articles/export-licensed-predator-makesmaiden- flight-400992/ [retrieved 09 July 2014].

[5] Boitz, C., "Global Hawk Maintainers Deliver ISR Capability to Warfighters," https://www.dvidshub.net/news/177042/global-hawk-maintainers-deliver-isr-capability-warfighters#.VgRJwDeFOM8 [retrieved 24 Sept. 2015].

[6] Daidzic, N. E., Piancastelli, L., and Cattini, A., "Diesel Engines for Light-to-Medium Helicopters and Airplanes (Editorial)," *International Journal of Aviation, Aeronautics, and Aerospace*, Vol. 1, No. 3, Jan. 2014, Paper 2, http://commons.erau.edu/ijaaa/vol1/iss3/2 [retrieved 02 Oct. 2016].

[7] "Continental CD-135 Data Sheet," Continental Motors, Technify Motors GmbH, Platanenstr, Germany, July 2014, http://continentaldiesel.com/typo3/index.php?id=59 [retrieved 18 July 2014].

[8] "ROTAX 915 IS/ISC Data Sheet," Rotax Aircraft Engines, BRP-Rotax GmbH & Co KG, Gunskirchen, Austria, Sept. 2015, http://www.flyrotax.com/produkte/detail/rotax-915-is-isc.html [retrieved 19 Oct. 2016].

[9] "VD Motor/Controller Packages," EVDrive Electric Motors, Portland, Oregon, Aug. 2012, http://www.evdrive.com/products/evd-motor-controller [retrieved 19 Oct. 2016].

[10] "W165FPTOT-18 Data Sheet," Winco Generators, Le Center, MN, Nov. 2000, http://www.wincogen.com/W165FPTOT-18 [retrieved 19 Oct. 2016].

[11] "Engine Certification Data," U.S. Environmental Protection Agency, Ann Arbor, MI, Aug. 2015, https://www3.epa.gov/otaq/certdata.htm [retrieved 27 July 2016].

[12] "Panasonic Develops New Higher-Capacity 18650 Li-Ion Cells," Green Car Congress, Mill Valley, CA, Dec. 2009, http://www.greencarcongress.com/2009/12/panasonic-20091225.html [retrieved 25 Dec. 2009].

[13] "International Civil Aviation Organization—Aircraft Engine Emissions Databank," European Aviation Safety Agency, Cologne, Germany, 2016, https://www.easa.europa.eu/document-library/icao-aircraft-engine-emissions-databank [retrieved 30 April 2016].

[14] Bauer, H., (ed.) *Automotive Handbook*, 8th ed., Ingram Book Group LLC, La Vergne, TN, 2011, p. 993.

[15] *Energy Loss and Efficiency of Power Transmission Belts*, Carlisle Power Transmission Products Inc., Belt Technical Center, Springfield, MO, 2009, pp. 1–10.

[16] *High Performance EVD Motor/Controller IP67 Drive Sub-Systems*, EVDrive Motors, EVDrive Research, Portland, Oregon, 2016, pp. 1–2.

[17] Höhn, B. R., Stahl, K., and Gwinner, P., "Light-Weight Design for Planetary Gear Transmissions," *Gear Technology*, Randall Publications, Elk Grove Village, IL, Sept. 2013, pp. 96–103.

[18] McCormick, B. W., *Aerodynamics, Aeronautics, and Flight Mechanics*, 1st ed., Wiley, New York, 1979, Chap. 6.

[19] Raymer, D. P., *Aircraft Design: A Conceptual Approach*, 2nd ed., AIAA, Washington, D.C., 1992, p. 20.

[20] Piancastelli, L., Frizziero, L., Pica, S., and Donnici, G., "High Altitude Operations with Piston Engines Power Plant Design Optimization, Part 1: Introduction," *ARPN Journal of Engineering and Applied Sciences*, Vol. 11, No. 5, March 2016, pp. 3525–3533.

[21] "Generalized Method of Propeller Performance Estimation," Hamilton Standard, Windsor Locks, CT, 1963, http://hdl.handle.net/2144/10454 [retrieved 16 Oct. 2016].

[22] Roskam, J., and Lan, C. T., *Airplane Aerodynamics and Performance*, Darcorporation, Lawrence, KS, 2016, pp. 643–683.

[23] Piancastelli, L., Frizziero, L., and Rocchi, I., "Feasible Optimum Design of a Turbocompound Diesel Brayton Cycle for Diesel-Turbo-Fan Aircraft Propulsion," *International Journal of Heat and Technology*, Vol. 30, No. 2, Dec. 2012, pp. 121–126. doi:10.18280/ijht

[24] "The Leap Engine. Performance. Execution. Technology," CFM International, Cincinnati, OH, Aug. 2012, https://www.cfmaeroengines.com/engines/leap [retrieved 12 Oct. 2016].

[25] Heywood, J. B., *Internal Combustion Engine Fundamentals*, 1st ed., McGraw–Hill, New Delhi, India, 1988, p. 503.

[26] Annand, W. J. D., "Heat Transfer in the Cylinders of Reciprocating Internal Combustion Engines," *Proceedings of the Institution of Mechanical Engineers*, Vol. 177, No. 36, 1963, pp. 973–996. doi:10.1243/PIME_PROC_1963_177_069_02

[27] Sookdeo, T., "Performance Measurement, Simulation, and Analysis of the Cox Tee Dee 0.010, the World's Smallest Production IC Engine," M.S. Thesis, Univ. of Maryland, College Park, MD, 2006.

[28] Dormand, J. R., and Prince, P. J., "A Family of Embedded Runge–Kutta Formulae," *Journal of Computational and Applied Mathematics*, Vol. 6, No. 1, 1980, pp. 19–26. doi:10.1016/0771-050X(80)90013-3

[29] White, F. M., *Viscous Fluid Flow*, McGraw–Hill, New York, 2006, pp. 411–480.

[30] Hall, D. K., Greitzer, E. M., and Tan, C. S., "Performance Limits of Axial Turbomachine Stages," *ASME Turbo Expo: Power for Land, Sea, and Air*, Vol. 8, Turbomachinery, Parts A, B, and C, Dept. of Aeronautics and Astronautics, Massachusetts Inst. of Technology, Boston, MA, 2011, pp. 479–489. doi:10.1115/GT2012-69709

[31] Sharma, O., and Butler, T., "Predictions of Endwall Losses and Secondary Flows in Axial Flow Turbine Cascades," *Journal of Turbomachinery*, Vol. 109, No. 2, 1987, pp. 229–236. doi:10.1115/1.3262089

[32] Denton, J., "The 1993 IGTI Scholar Lecture: Loss Mechanisms in Turbomachines," *Journal of Turbomachinery*, Vol. 115, No. 4, Oct. 1993, pp. 621–656. doi:10.1115/1.2929299

[33] Sirignano, W. A., and Liu, F., "Performance Increases for Gas-Turbine Engines Through Combustion Inside the Turbine," *Journal of Propulsion and Power*, Vol. 15, No. 1, 1999, pp. 111–118. doi:10.2514/2.5398

[34] Liu, F., and Sirignano, W. A., "Turbojet and Turbofan Engine Performance Increases Through Turbine Burners," *Journal of Propulsion and Power*, Vol. 17, No. 3, 2001, pp. 695–705. doi:10.2514/2.5797

[35] Sirignano, W. A., Dunn-Rankin, D., Liu, F., Colcord, B., and Puranam, S., "Turbine Burners: Performance Improvement and Challenge of Flameholding," *AIAA Journal*, Vol. 50, No. 8, 2012, pp. 1645–1669. doi:10.2514/1.J051562

J. P. Bons
Associate Editor